RSC Advances

ROYAL SOCIETY OF CHEMISTRY

www.rsc.org/advances

Graphical Abstract

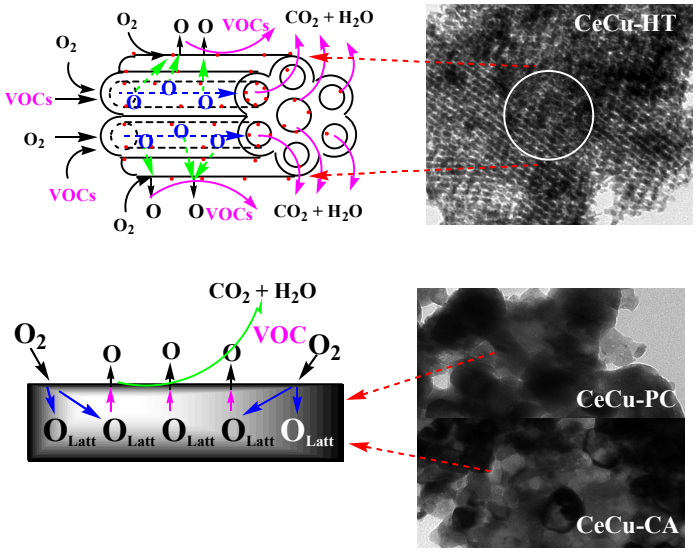

CeCu-HT, CeCu-PC, and CeCu-CA catalysts were prepared and used in phenyl VOCs catalytic combustion in air. The CeCu-HT catalyst exhibits high phenyl VOCs catalytic combustion activity, which can be attributed to the CeCu-HT catalyst having ordered bicontinuous mesoporous structure and high specific surface area. The structure characteristics facilitate the adsorption and activation of the reactant molecules on the outer and inner surface, which can improve phenyl VOCs catalytic combustion reaction. The adsorption and activation of the reactant molecules mainly take place on the outer surface of the CeCu-PC, and CeCu-CA catalysts for the bulky and piled structure. The CeCu–HT catalyst had high activities and stabilities for ethylbenzene catalytic combustion.

Effects of preparation method on CeCu oxide catalyst performance

Guilin Zhou*, Hai Lan, Ruyi Song, Hongmei Xie, Qinxiang Du

Key Laboratory of Catalysis Science and Technology of Chongqing Education Commission, Department of Chemistry and Chemical Engineering, Chongqing Technology and Business University, Chongqing 400067, China

* To whom all correspondence should be addressed

E-mail address: upcglzhou@sohu.com or dicpglzhou@ctbu.edu.cn (Guilin Zhou);

Tel.: +86-23-62769076; Fax: +86-23-62769785-605

Abstract: CeCu–HT, CeCu–PC, and CeCu–CA composite oxide catalysts were synthesized using hard-template, coprecipitation, and complex methods, respectively, were characterized by XRD, TEM, BET, XPS, and H_2–TPR. Catalytic properties were investigated through the catalytic combustion of phenyl volatile organic compounds in air. XRD results show that the prepared CeCu oxide catalysts all had CeCu oxide solid solution phases but distinct crystallinities and phase components. Low-angle XRD, TEM, and BET results demonstrate that CeCu–HT had a developed and ordered bicontinuous mesoporous structure, as well as a large specific surface area of 206 $m^2 \cdot g^{-1}$. CeCu–PC and CeCu–CA formed low-porosity, agglomerated structures with specific surface areas of 15 and 24 $m^2 \cdot g^{-1}$, respectively. XPS results confirm that main chemical valance of the Ce and Cu species in the prepared CeCu catalysts is +4 and +2, respectively. And combining with H2–TPR, CeCu–HT had more active oxygen species and higher reducibility compared with CeCu–PC and CeCu–CA. CeCu–HT had higher phenyl VOCs catalytic combustion activity in air than CeCu–PC and CeCu–CA, and follow the following activity order: ethylbenzene > toluene > xylene > benzene. The prepared catalysts had low benzene catalytic combustion activities, with conversion below 70% in the studied temperature range. Lifetime test results show that the catalysts had high stabilities for ethylbenzene catalytic combustion because of their efficient activation of oxygen molecules from air to form active oxygen species at the corresponding temperature. The clear differences between the phenyl VOC catalytic combustion performances of the three CeCu oxide catalysts can be attributed to their distinct chemical components and

structures, as well as to the physicochemical properties of phenyl VOC molecules.

***Keywords*:** CeCu oxide catalyst; Ordered mesopores; Active oxygen species; Catalytic combustion; Phenyl VOCs

1 Introduction

Volatile organic compounds (VOCs) are recognized as a major source of air pollution. A typical type of VOCs is phenyl VOCs, of which benzene, toluene, xylene, and ethylbenzene are the primary representatives.[1] These compounds have a wide range of applications and are generally used as starting materials and organic solvents for a large number of chemical industries. However, these phenyl VOCs are toxic to the central nervous system and can cause cancer in humans. In addition, these compounds are closely related to atmospheric photochemical smog and aerosol. This type of pollution has become a critical global issue that requires efficient techniques that utilize environmental treatment systems. Among of these used techniques, catalytic combustion technology has been found to be a new, effective, and economical approach to removing VOCs. Catalytic combustion can achieve complete catalytic oxidation by converting VOCs into CO_2 and H_2O with low energy consumption. More importantly, this technique can be used in diluted effluent streams (<1.0 vol% VOCs). However, the primary application of catalytic combustion is the design and development of high-performance catalytic materials. Transition metals such as Mn, Cu, Ce, and Co, which are naturally abundant and rich in extranuclear *d*–shell electrons, have excellent catalytic properties.[2–4] These transition metals are usually prepared into composite metal oxide catalysts because single-metal oxide catalysts exhibit low thermal stability and low catalytic activity in VOC catalytic combustion.

CeCu bimetal oxide systems have been intensively studied in various reactions,

such as water–gas shift, preferential CO oxidation, methanol oxidative steam reforming, N_2O decomposition and acetone and methane combustion.[5–10] However, CeCu oxide catalysts prepared by traditional methods, such as coprecipitation, deposition–precipitation and complexation–combustion, have limited catalytic performances[5,7]. Moreover, these reported CeCu oxide catalysts generally have low specific surface areas and porosities, as well as large CuO particles and agglomerates even at low Cu contents, resulting in small interphase surface areas. One way of increasing the specific surface areas of CeCu oxide catalysts and improving CuO dispersion is the application of novel preparation methods. Hard-template synthesis reportedly yields catalysts with the aforementioned properties.[11] KIT–6, which has a cubic *Ia3d* structure (with three-dimensionally ordered mesopore arrays and a large pore volume), can be used as a thermally stable and highly porous template; it is reportedly one of the most preferred among mesoporous silica materials.[12,13] However, the use of these KIT–6–derived CeCu oxide catalysts in VOCs catalytic combustion has been rarely reported. The factors affecting the catalytic properties of CeCu oxide catalysts in phenyl VOC catalytic combustion require further investigation. Therefore, the synthesis of CeCu composite oxide catalysts using different methods to catalytically eliminate phenyl VOCs from air is highly important for environmental protection and for the identification of alternative catalytic materials.

The current study aims to synthesize CeCu composite oxide catalysts with superior structural properties and compositions. The prepared CeCu oxide catalysts were characterized by X-ray diffraction (XRD), transmission electron microscopy

(TEM), Brunauer–Emmett–Teller (BET) analysis, and X-ray photoelectron spectroscopy (XPS), their catalytic performances were also investigated by the phenyl VOCs (benzene, toluene, xylene, and ethylbenzene) catalytic combustion in air.

2. Experimental

2.1 Catalyst preparation

In a typical synthesis of mesoporous CeCu composite oxide catalyst by the hard–template method, 1.0 g each of $Ce(NO_3)_3{\cdot}6H_2O$ and $Cu(NO_3)_2{\cdot}3H_2O$ (Ce/Cu molar ratio = 3.0) was dissolved in 20 mL of ethanol. KIT–6 mesoporous silica was then added. The silica template was prepared according to the procedure described by Ryoo et al..[14] The mixture was stirred at room temperature until a dry powder was obtained. The powder was then slowly heated to 400 °C and calcined at that temperature for 2.0 h. The impregnation procedure was repeated, followed by calcination at 500 °C for 3 h. The resulting samples were treated three times with 2 M NaOH to remove the silica template. Afterwards, the samples were centrifuged, washed several times with water and ethanol, and then dried at 100 °C in air. The obtained product was designated as CeCu–HT.

In a typical complex–method synthesis of CeCu composite oxide catalyst, $Cu(NO_3)_2{\cdot}3H_2O$, $Ce(NO_3)_3{\cdot}6H_2O$, and citric acid (CA) (Ce/Cu molar ratio = 3.0; CA/(Ce+Cu) molar ratio = 1.8) were dissolved in a certain amount of deionized water. The mixture was then stirred at 80 °C until the deionized water completely evaporated. Afterwards, the sample was dried in an oven at 90 °C for 24 h, slowly heated to

500 °C, and calcined at that temperature for 3 h. The CeCu composite oxide catalyst was then obtained and designated as CeCu–CA.

In a typical co–precipitation synthesis of CeCu oxide catalyst, $Cu(NO_3)_2{\cdot}3H_2O$, $Ce(NO_3)_3{\cdot}6H_2O$ (Ce/Cu molar ratio = 3.0) were dissolved in a certain amount of deionized water. The mixed solution was stirred at room temperature, and dilute ammonia water was then added dropwise in the mixture until the pH of the solution reaching to 9.0. The obtained precipitate was thoroughly washed with distilled water in ordered to remove the undesired NH_4^+ ions, and subsequently dried overnight in an oven at 100 °C. The dried sample was calcined at 500 °C for 3 h, and the obtained CeCu oxide catalyst sample is referred to as CeCu–PC.

2.2 Catalyst characterization

2.2.1 XRD characterization

X–ray diffraction (XRD) patterns were recorded on a Rigaku D/Max–2500/PC diffractometer with a rotating anode using Ni filtered Cu–Kα (as radiation source (λ = 0.15418 nm) radiation at 40 kV of a tube voltage and 200 mA of a tube current. The data of 2θ from 20° to 80° range were collected with the step size of 0.02°at the rate of 5°/min. Low-angle XRD data was corrected form 0.5° to 5° with 0.02° increment and recording time of 100 s at each increment.

2.2.2 TEM analysis

Transmission electron microscopy (TEM) was performed using a Tecnai G^2 Spirit microscope operating with an acceleration voltage of 120 kV. For the TEM measurement, the samples were prepared by ultrasonication in ethanol, evaporating a drop of the resultant suspension onto a carbon–coated copper grid.

2.2.3. BET characterization

Adsorption and desorption isotherms were collected on Autosorb–6 at -196 °C. Prior to the measurement, all samples were degassed at 200 °C until a stable vacuum of ca. 5 mTorr was reached. The specific surface area of the CeCu–HT, CeCu–PC, and CeCu–CA catalysts, as calculated from the BET equation, are 206, 15, and 24 $m^2 \cdot g^{-1}$, respectively.

2.2.4 XPS and AAS analysis

The chemical states of Ce, Cu and O in the prepared CeCu oxide catalysts were certified by the X–ray photoelectron spectroscopy (XPS) measurements. The signals were collected by a KRATOS X–ray sources with an aluminium crystal, operating at 12 kV anode voltage and 12 mA emission current, was used to generate the required Al *K*α radiation. Curve fitting and background subtraction were performed using Casa XPS software. Atom adsorption spectrum (AAS) was performed on a Z-5000 type polarized zeeman atomic absorption spectrophotometer.

2.2.5 H_2-TPR studies

H_2 temperature programmed reduction (H_2–TPR) was conducted using a conventional apparatus equipped with a TCD detector. 15 mg of sample was placed in a quartz tube (4.0 mm ID), and then H_2–TPR was performed by heating the samples at 10 °C·min^{-1} from 30 to 700 °C in a 5% H_2–Ar mixture flowing at 25 ml·min^{-1}.

2.3. Catalytic activity measurement

Catalytic tests of all catalysts were carried out in a continuous flow fixed–bed quartz tubular reactor (i.d. 6 mm) under atmospheric pressure. The quartz tube reactor containing 50 mg catalyst was placed inside a tubular furnace. The air, which contains

gaseous phenyl VOCs (benzene, toluene, xylene, or ethylbenzene) (1.0 vol.%), was passed downward through the reactor containing the catalyst bed with a gas mass space velocity of 66,000 $mL \cdot g^{-1} \cdot h^{-1}$. Catalytic activity tests were performed at given temperature, and the reaction temperature was monitored by a temperature programmable controller (ÜGU, model 708P, China). The quantity of phenyl VOCs in the feed gas and reaction products gas were monitored by using on–line gas chromatograph (GC 6890II), equipped with a FID.

3. Results and Discussion

3.1 XRD characterization

The XRD patterns of the prepared CeCu–CA, CeCu–PC, and CeCu–HT catalysts are shown in Fig. 1. The XRD patterns of CeCu–CA and CeCu–PC both show eight intense and sharp diffraction peaks associated with the fluorite-like structure of the CeO_2 crystalline phase, and additional two relatively weak diffraction peaks attributed to the CuO crystalline phase.[15,16] Meanwhile, the XRD peaks of CeCu–PC are relatively weaker and broader than those of CeCu–CA. By contrast, the XRD peaks of the CuO crystalline phase in the CeCu–PC XRD pattern are stronger and more highlighted than those of the CeCu–CA catalyst. However, the CeCu–HT XRD pattern only shows four weak and broad diffraction peaks corresponding to the CeO_2 crystalline phase with a fluorite-like structure. When 2θ exceeds 60°, the diffraction peaks of the CeO_2 crystalline phase nearly disappear, corresponding to those in the patterns of the CeCu–CA and CeCu–PC catalysts. The CeO_2 XRD peaks

of the CeCu–HT catalyst clearly shift to the large 2θ.[7,15] And no XRD peaks corresponding to the CuO crystalline phase are observed for CeCu–HT. Moreover, diffraction peaks ascribed to the Cu_2O crystalline phase are not observed.

The solubility product constants of $Ce(OH)_3$ and $Cu(OH)_2$ in aqueous solutions are 1.6×10^{-20} and 2.2×10^{-20}, respectively. Given the solubility product constant difference, a homogeneous precipitation that yields isolated $Ce(OH)_3$ and $Cu(OH)_2$ precipitates cannot be completely achieved. Therefore, the generated CuO cannot be fully dissolved into the CeO_2 lattice under high-temperature calcination, which leads to the formation of a large amount of isolated crystalline CuO species in the CeCu–PC catalyst. The high-intensity XRD peaks of crystalline CeO_2 and the weak XRD peaks of crystalline CuO indicate that aside from the CeCu oxide solid solution, a large number of isolated crystalline CeO_2 species and a certain amount of crystalline and amorphous CuO species coexist in the CeCu–CA catalyst. For the CeCu–CA catalyst, the complex methods promote the even distribution of the Cu species in the catalyst system, which in turn promotes the formation of well-dispersed CuO species by high-temperature calcination. The presence of a large number of isolated crystalline CeO_2 can be attributed to the loss of Cu species during high-temperature calcination, leading to the formation of a small amount of CeCu oxide solid solution and a large amount of isolated CeO_2 with perfect crystalline phase in the prepared CeCu–CA catalyst.[17]

In the CeCu–HT catalyst system, only the weak and wide XRD peaks of the CeCu oxide solid solution phases are observed; the XRD peaks of the crystalline CuO

phases are not found. In addition, the positions of the CeCu oxide solid solution diffraction peaks clearly shift to high 2θ values. The weak and wide peaks can be attributed to the destruction of the CeO_2 lattice integrity because of the incorporation of CuO species into the CeO_2 lattice to form the CeCu oxide solid solution. In the CeCu oxide solid solution, some of Ce^{4+} ions can be substituted by the Cu^{2+} ions. This phenomenon results in decreased CeO_2 lattice parameters because of the smaller radius of Cu^{2+} ions (0.072 nm) compared with that of Ce^{4+} ions (0.097 nm) and leads to the shifting of the CeO_2 XRD peaks to high 2θ values.[7] In the CeCu–HT catalyst, the CuO species can fully dissolve into the CeO_2 lattice because of the ordered mesoporous structure of the hard template KIT–6. The Cu and Ce species are encapsulated in the KIT–6 mesoporous structure, which promotes the mixing of the Cu and Ce precursors at the atomic level. Simultaneously, the space-confining effects of the KIT–6 nanopores limit the diffusion, migration, and grain growth of the Cu and Ce species during catalyst preparation. The interaction between CuO and CeO_2 species is also promoted, resulting from the full incorporation of CuO into the CeO_2 lattice to form the CeCu oxide solid solution.[13]

In the CeCu oxide catalysts, the Ce–O–Cu chemical bonds, rather than the simple Ce–O and Cu–O chemical bonds, exist in the CeCu composite oxide. This Ce–O–Cu bond results from the formation of a large amount of CeCu oxide solid solution, thus promoting the strong interaction between CuO and CeO_2. Therefore, the metal–oxygen chemical bonds of the CeCu composite oxide system are the modified Ce–O and Cu–O chemical bonds, which lead to changes in the chemical properties. In

addition, CuO species are incorporated into the CeO_2 crystallite lattice to form the CeCu oxide solid solution. The substitution of Cu^{2+} ions for segmental Ce^{4+} ions in the CeO_2 crystallite lattice creates a charge imbalance. As a result, large amounts of structural defects, also called oxygen vacancies, are generated to restore the charge balance in the CeCu oxide solid solution. These oxygen vacancies can serve as adsorption and activation sites for oxygen molecules.[3] The large amounts of adsorbed oxygen species can effectively promote the movement of oxygen species among the oxides in the solid solution catalyst and generate a significantly higher amount of reactive oxygen species, which leads to significantly improved catalytic oxidation or combustion performance.

As shown in Fig. 1, the low-angle XRD peaks of the CeCu–CA and CeCu–PC catalysts are not observed at the 0.5° to 5.0° range. However, the KIT–6 template and CeCu–HT exhibit a sharp, intense, low-angle XRD peak at 2θ =0.98° belonging to the reflection from the {211} crystalline plane[11]. This result confirms the prepared CeCu–HT catalyst has a well-ordered mesoporous structure and belongs to the *Ia3d* bicontinuous cubic symmetry space group.[18,19]

3.2 TEM analysis

The TEM images of the prepared CeCu–HT, CeCu–PC, CeCu–CA catalysts, and KIT–6 template are shown in Fig. 2. The prepared CeCu–HT catalyst exhibits a developed mesoporous structure with a pore size of approximately 5 nm to 6 nm and a pore wall thickness of approximately 8 nm. These properties are characteristic of mesoporous oxide catalysts. The prepared CeCu–PC catalyst exhibits a bulky,

disorderly, piled structure. Furthermore, the particles are large and closely packed, and the particle diameters range from approximately 60 nm to 300 nm. Meanwhile, the prepared CeCu–CA catalyst exhibits loosely aggregated structures with distinct particle sizes between 20 and 60 nm, which are clearly significantly smaller than those of CeCu–PC. Moreover, the TEM images of both CeCu–PC and CeCu–CA show no apparent porous structure.

The CeCu–PC catalyst was prepared using the conventional coprecipitation method. Therefore, catalyst particle growth cannot be controlled and effectively limited, and massive, large-diameter particles with distinct sizes and shapes are generally obtained. By contrast, the CeCu–CA catalyst was prepared using a citric acid complex method, in which citric acid complexes with Ce^{3+} and Cu^{2+} form stable gel precursors. Gases such as CO_2, NO_x, and water vapor are produced by citric acid and NO^{3-} thermal decomposition during the high-temperature calcination of dried gel precursors. In this procedure, the large amount of gas produced and released leads to the formation of a loose catalyst structure, and the obtained particle diameters are relatively small. However, the complex method does not promote the formation of a porous structure, and the obtained particles tend to form aggregates with different sizes.[17]

Based on the Fig.2 and low-angle XRD results, the KIT–6 template has an ordered mesoporous structure with three-dimensional symmetry. The most diameters of the pores fall between 5.9 and 8.6 nm, with the maximum at 7.0 nm.[19] The KIT–6 template shows a vital function to porous structure formation and pore size adjustment.

The porous structure of the prepared CeCu–HT catalyst can be associated with the KIT–6 skeletal structure, whereas the skeletal structure of the prepared CeCu–HT catalyst can be related to the porous structure of the KIT–6 hard template. Therefore, catalysts with developed porous structures can be prepared using the hard-template method. The TEM results in Fig. 2 show that the CeCu–HT catalyst forms an ordered mesoporous structure that is highly similar to that of the KIT–6 template. This ordered mesoporous structure is completely different from those of the CeCu–PC and CeCu–CA catalysts, which have large aggregated structures. These results are also confirmed by low-angle XRD analysis. However, the surface active components and the interactions between components can usually be affected by the microscopic structures of the CeCu composite oxide catalysts .[2,3] Therefore, CeCu–HT, CeCu–PC, and CeCu–CA may have significantly different catalytic activities as a result of differences in their structural performances.

3.3 XPS and AAS studies

Fig. 3 shows the detailed XPS characterization results for the CeCu–PC, CeCu–CA, and CeCu–HT catalysts synthesized using different preparation methods. The Ce 3d XPS spectra of the prepared samples are shown in Fig. 3a. Six highly observable XPS peaks at binding energies of approximately 882.4, 888.2, 898.1, 900.5, 907.2, and 916.4 eV are found in the Ce 3d XPS spectra of the CeCu–PC, CeCu–CA, and CeCu–HT catalysts. The principal XPS peaks located at approximately 882.5 and 900.5 eV are ascribed to Ce 3d3/2 and Ce 3d5/2, respectively. The peaks at the binding energies of approximately 907.4/916.7 and

888.4/898.1 eV are satellites arising from Ce 3d3/2 and Ce 3d5/2, respectively.[7,9] This result is consistent with that of a previous report on Ce^{4+}, indicating that the main chemical valence of the Ce species is +4 on the surface of the prepared CeCu oxide catalysts and that the Ce species should be CeO_2.[9]

Fig. 3b shows the Cu 2p XPS spectra of the prepared CeCu–PC, CeCu–CA, and CeCu–HT catalysts. Four prominent XPS peaks are observed at binding energies of approximately 933.7, 941.4, 953.3, and 961.5 eV. The XPS peaks centered at 933.7 and 953.3 eV correspond to Cu 2p3/2 and Cu 2p1/2, respectively. The peaks located at 941.4 and 961.5 eV are corresponding satellites arising from Cu 2p1/2 and Cu 2p3/2, respectively. The high Cu 2p3/2 binding energy (933.0 eV to 933.9 eV) and shake-up peak (939 eV to 944 eV) are two major XPS characteristics of Cu^{2+}.[7,9,13] The Cu2p3/2 XPS peak centered at 933.8 eV and the corresponding shake-up peak at approximately 941.9 eV are observed in the XPS spectra of the CeCu–PC, CeCu–CA, and CeCu–HT catalysts, indicating that the Cu species initially present in these samples are mainly in a divalent chemical oxidation state. The detailed XPS results (Table 1) indicate that the surface Ce/Cu molar ratio on the CeCu–PC, CeCu–CA, and CeCu–HT catalysts are 1.89, 2.06, and 1.84, respectively, indicating that the preparation methods significantly affect the surface Cu species content of the prepared CeCu-oxide solid solution catalysts. The surface Ce/Cu molar ratio on the CeCu–PC, CeCu–CA, and CeCu–HT catalysts are significantly lower than the values of 8.55, 3.21, 3.53 according to the results (Table 1) measured by AAS, which can be attributed to the enrichment of the Cu species on the surface of the CeCu oxide solid

solution catalysts.[5] However, the Ce/Cu molar ratio in the prepared samples is higher than the 3.0 value of the initial metal dosage, especially for the CeCu–PC catalyst, which can be attributed to the loss of the Cu species in the process of the catalysts preparation. The Ce/Cu molar ratio in the CeCu-PC exceeds 8.5 indicating that the Cu content badly reduces in the CeCu–PC catalyst, which can be attributed to the $Cu(OH)_2$ deposition being further dissolved by the ammonia water during the precipitation progress. These qualitative and quantitative analytical results indicate that the preparation methods are vital to the chemical composition and distribution of active components on the surface of CeCu oxide solid solution catalysts.

Fig. 3c shows the O 1s XPS spectra of the CeCu–PC, CeCu–CA, and CeCu–HT catalysts. By scientifically resolving the highly asymmetric O 1s XPS spectra, three XPS peaks of the CeCu–PC, CeCu–CA, and CeCu–HT catalysts are observed about binding energies of 529.3, 531.0, and 532.3 eV. The resolved peak centered at 528.9 eV to 529.5 eV is ascribed to the catalyst surface lattice oxygen, the resolved peak with binding energy of 529.7 eV to 531.5 eV is assigned to surface adsorption oxygen O_2^{2-} or O^-, and the resolved peak at a high binding energy of 531.5 eV to 532.5 eV corresponds to hydroxyl oxygen OH^-.[23,24] The surface lattice oxygen contents of CeCu–PC, CeCu–CA, and CeCu–HT are 63.8%, 64.7%, and 52.7%, respectively, as shown in the XPS analysis results in Table 1. The surface adsorption oxygen contents of CeCu–PC, CeCu–CA, and CeCu–HT are 29.0%, 28.0%, and 33.1%, respectively. CeCu–PC and CeCu–CA have similar lattice oxygen contents, which are obviously higher than the CeCu-HT. CeCu–PC has slightly high adsrption

oxygen content compared with CeCu–CA, whereas CeCu–HT has higher adsorption oxygen content than the other samples. In the CeCu–HT oxide catalyst, a significantly higher amount of CuO species are fully dissolved into the CeO_2 lattice to form a large amount of CeCu oxide solid solution. Therefore, the synergic effects and interactions between CuO and CeO_2 are significantly enhanced, whereas the Ce–O and Cu–O chemical bonds are weakened, resulting in the efficient conversion of the lattice oxygen species into adsorbed active oxygen species.[8] At the same time, the significantly higher amount of CeCu oxide solid solution forms considerably more changes in the lattice structure and results in the production of more lattice defects in the catalyst. In turn, the oxygen vacancies in the CeCu–HT catalyst increase, thus improving the adsorption amount and capacity of this catalyst for oxygen molecules.[9] The existence of large amounts of adsorption oxygen on the catalyst surface can produce abundant active oxygen species that contributes to the high activity of the catalysts in the combustion reaction of VOCs.

3.4 H_2–TPR studies

The reducibilities of the prepared CeCu oxide solid solution catalysts were characterized using H_2–TPR, and the profiles are shown in Fig. 4. The H_2 consumption curve of the CeCu–HT catalyst deviates from the baseline (as shown by the arrow) at approximately 120 °C. In addition, two clear H_2 consumption peaks, α and β, are observed at 195 and 214 °C, respectively. The intensity and area of peak β are significantly greater than those of peak α. Meanwhile, the H_2 consumption curve of the CeCu–PC catalyst deviates from the baseline up to 160 °C. In addition, two

clear H_2 consumption peaks, α and β, are observed at 222 and 244 °C, respectively, when the reduction temperature is increased. The CeCu–PC and CeCu–HT catalysts have two similar H_2–TPR peaks. However, the H_2–TPR peak temperatures of the CeCu–PC catalyst are significantly higher than those of the CeCu–HT catalyst, whereas its H_2 consumption peaks are relatively weak and wide. For the CeCu–CA catalyst, the H_2 consumption curve deviates from the baseline at approximately 130 °C (as shown by the arrow). In addition, three clear H_2 consumption peaks, namely, γ, α and β, are observed at 159, 192, and 218.5 °C, respectively. The intensity and area of β are significantly greater than those of γ and α. At the same time, the H_2 consumption peaks of the CeCu–CA catalyst are weaker and wider compared with those of the CeCu–HT and CeCu–PC catalysts. Moreover, the H_2 consumption peaks of the three catalysts all occur in the reduction temperature range below 280 °C. The CeCu–HT catalyst has significantly lower H_2 consumption peak temperatures than CeCu–CA and CeCu–PC.

Generally, pure CuO prepared through conventional method has H_2 consumption peak at approximately 300 °C, and pure CeO_2 prepared by conventional methods exhibits two H_2 consumption peaks at approximately 450 and 900 °C, respectively.[6,8,10] Therefore, the H_2–TPR reduction peaks of the CeCu–HT, CeCu–CA, and CeCu–PC catalysts are all below 300 °C, which can be mainly attributed to the reduction of the CuO species in the catalysts. The different H_2–TPR reduction peaks indicate that the CuO species exists in different forms in the CeCu oxide catalysts prepared by different methods. The H_2 consumption peak α of the three composite

oxide catalysts at low temperatures can be attributed to the reduction of the highly dispersed CuO species and/or to the strong interaction between the CuO species and the CeO_2 on the surface of the prepared CeCu oxide catalysts. The high-intensity H_2 consumption reduction peak β can be attributed to the reduction of the reducible species, which contains the Cu^+ species formed by the reduction of the Cu^{2+} species at low temperatures, as well as to the strong interaction between the CuO species and CeO_2 in the bulk of the CeCu composite oxide catalysts and to the highly dispersed crystalline CuO species in the catalysts.[6,9] In addition, the highly dispersed CeO_2 species strongly interacts with CuO which exists on the surface of the CeCu composite oxide catalysts. This phenomenon may also have contributed to the H_2 consumption reduction peak β at high temperature. As the XRD results indicate, a large amount of CeCu oxide solid solution is present in the prepared CeCu oxide catalysts. The existing Ce–O–Cu chemical bonds in the CeCu oxide solid solution can significantly promote the movement of the oxygen species between CuO and CeO_2 during the reduction process. As a result, when the Cu^{2+} species is reduced to Cu^+ by H_2 during the reduction, the low-valence state Cu^+ can be reoxidized to Cu^{2+} by the Ce^{4+} species, which has a high valance state. The process achieves oxygen species transfer between CeO_2 and CuO, which also promotes the reduction of Ce^{4+} to Ce^{3+} at low temperatures. For the CeCu–CA catalyst, H_2 consumption reduction peak γ is observed at low temperatures in addition to the H_2 consumption reduction peaks α and β. The formation of the extra peak γ can be attributed to the low-crystallinity, superfine CuO nanoparticles with high low-temperature reducibility. These

nanoparticles are formed from the complex citric acid-promoted dispersion of CeO_2 and CuO, as well as from the formation of superfine CuO nanoparticles during high-temperature calcination.[17]

As shown in Fig. 4, the H_2–TPR reduction peak temperatures of the CeCu–HT, CeCu–CA, and CeCu–PC catalysts are clearly lower than those of the pure CuO or CeO_2 species, indicating that the reducibility of the oxides (CuO and CeO_2) in the prepared CeCu oxide solid solutions can be significantly improved. This can be attributed to the strong interaction between CuO and CeO_2 in the CeCu oxide catalysts weakening the Ce–O and Cu–O chemical bonds.[6,18] XRD and XPS characterization results show that aside from the CeCu oxide solid solution, a large amount of highly dispersed amorphous CuO species and a certain amount of highly crystalline CuO species are also present in the CeCu–CA and CeCu–PC catalysts, respectively. Highly dispersed amorphous transition metal oxides generally have high reducibility.[7] The CeCu–CA catalyst showing lower H_2–TPR reduction peak temperature than the CeCu–PC catalyst can be attributed to the presence of a large number of isolated and highly dispersed amorphous CuO.

The low-angle XRD, TEM, and BET results all indicate that the CeCu–HT catalyst has an ordered developed mesoporous structure and a large specific surface area, which result in the more facile reaction of H_2 molecules with the metal oxides in the CeCu–HT catalyst and lead to higher reduction performance of the CeCu–HT catalyst. The XRD results also confirm that CeCu–HT metal oxides have low crystallinity and higher amount of CeCu oxide solid solution than the CeCu–CA and

CeCu–PC catalysts, which allows the reduction of CeCu–HT catalyst at low temperatures. Therefore, the CeCu–HT catalyst shows high low-temperature reducibility, and its H_2–TPR reduction peak temperatures are significantly lower than those of the CeCu–CA and CeCu–PC catalysts. Moreover, the Cu–O and Ce–O chemical bonds of the CeCu oxide solid solution catalyst are effectively weakened, thus promoting the formation of reactive oxygen species.[18] Based on the XPS results, the CeCu–HT catalyst has the highest reactive oxygen species content among the prepared CeCu oxide catalysts, thus further confirming the high low-temperature reducibility of this catalyst. This result indicates that the CeCu–HT catalyst can provide a large number of reactive oxygen species for catalytic oxidation or combustion reactions.

3.5 Determination of phenyl VOC catalytic combustion activity

The relationships between the reaction temperature and the catalytic combustion conversion of the phenyl VOCs are shown in Figs. 5a to 5c, respectively. The results show that the CeCu–HT, CeCu–PC, and CeCu–CA catalysts all exhibit high catalytic combustion activity for benzene, toluene, xylene, and ethylbenzene. For the CeCu–HT catalyst, the minimum reaction temperatures at which toluene, xylene, and ethylbenzene conversions exceed 90% (T_{90}) and benzene conversion exceeds 60% (T_{60}) are 225, 240, 220, and 220 °C, respectively. The phenyl VOC catalytic combustion activity on the CeCu–HT catalyst follows the order ethylbenzene > toluene > xylene > benzene. The T_{90} for toluene, xylene, and ethylbenzene over the CeCu–PC catalyst reach 240, 245, and 225 °C, respectively. Moreover, the T_{60} of

benzene over the CeCu–PC catalyst is 245 °C. The phenyl VOC catalytic combustion activity on the CeCu–PC catalyst follows the order toluene > xylene > ethylbenzene > benzene. Meanwhile, for the CeCu–CA catalyst, the T_{90} for toluene and xylene are 240 and 295°C, respectively. The T_{60} of ethylbenzene and benzene over the CeCu–CA catalyst reach 245 and 290°C, respectively. These results indicate that phenyl VOC catalytic combustion activity on the CeCu–HT catalyst is higher than those on the CeCu–PC and CeCu–CA catalysts. However, the catalytic combustion removal of benzene on the CeCu–HT, CeCu–PC, and CeCu–CA catalysts is low and does not exceed 70%. At the same time, the catalytic combustion activity for phenyl VOCs over the CeCu–HT catalyst is clearly higher than those of precious metal catalysts Pd, Ru, and Pt.[25-28] These results indicate that this inexpensive and efficient CeCu–HT catalyst can be readily applied for the elimination of phenyl VOCs from air.

As shown in Fig. 5, the catalytic combustion temperatures for toluene, xylene, ethylbenzene, and benzene over the CeCu–HT catalyst are significantly lower than those over the CeCu–PC and CeCu–CA catalysts, indicating higher catalytic combustion activity of the CeCu–HT catalyst for phenyl VOCs. The catalytic performance of the catalysts in VOC combustion is a comprehensive property determined by the chemical composition and structure of the catalysts, which can be directly controlled and improved by the preparation method. Superior chemical composition and structure are the primary foundation for the effective removal of low-concentration phenyl VOCs by catalysts at low energy consumption. The XPS results show that Cu^{2+} and Ce^{4+} species exist on the surface of the CeCu–HT,

CeCu–PC, and CeCu–CA catalysts without forming low-chemical value Cu^{+} and Ce^{3+} species. The XRD results show that CuO has fully dissolved into the CeO_2 lattice to form the CeCu oxide solid solution in the CeCu–HT catalyst, whereas certain amounts of crystalline CuO species and CeCu oxide solid solution are present in the CeCu–PC and CeCu–CA catalysts. Therefore, the Ce–O and Cu–O chemical bonds are fully weakened and broken more easily to form the reactive oxygen species. At the same time, the integrity of the CeO_2 lattice in the CeCu oxide solid solution is destroyed and oxygen vacancies are generated, thus disrupting the charge balance. The generated oxygen vacancies in the CeCu–HT catalyst promote high adsorption and activation of oxygen molecules. Moreover, the movement and transfer of oxygen species in the catalysts can be significantly promoted by the existing adsorbed reactive oxygen species. By contrast, the isolated CuO species in the CeCu–PC and CeCu–CA catalysts indicate that CuO is not well dissolved in the CeO_2 lattice, thus negatively affecting the interaction between CuO and CeO_2. This phenomenon directly results in slightly weakened metal–oxygen chemical bonds, which leads to the formation of a limited amount of oxygen vacancies in the CeCu–PC and CeCu–CA catalysts. As a result, the adsorption and activation abilities of these catalysts for gas molecules are impaired, and their ability to provide active oxygen species for catalytic combustion is reduced. The XPS results confirm that the CeCu–HT catalyst has significantly higher adsorbed oxygen species content than the CeCu–PC and CeCu–CA catalysts, indicating that the CeCu–HT catalyst can provide more reactive oxygen species for the catalytic combustion reaction. A comparison of Figs. 5b and 5c

shows that the catalytic combustion temperatures of ethylbenzene, toluene, xylene, and benzene over the CeCu–PC catalyst are lower than those over the CeCu–CA catalyst. This result indicates that the CeCu–PC catalyst has higher phenyl VOC catalytic combustion performance than the CeCu–CA catalyst. This may be attributed to that the CeCu–PC catalyst has more adsorbed oxygen species than the CeCu–CA catalyst, as confirmed by the XPS results. Furthermore, the highly crystalline CeO_2 phase maintains its intact crystal structure and hinders the formation of oxygen vacancies in the CeCu–CA catalyst, thus reducing the activation ability of the CeCu–CA catalyst for O_2 gas molecules. As a result, the CeCu–CA catalyst cannot supply sufficient reactive oxygen species for phenyl VOC catalytic combustion at relatively low reaction temperatures. Therefore, the differences in the catalytic performances of the CeCu–HT, CeCu–PC, and CeCu–CA catalysts can be attributed to the distinct active components of the CeCu–HT, CeCu–PC and CeCu–CA catalysts.

As confirmed by the low–angle XRD, TEM, and BET results, the CeCu–HT catalyst has a developed and ordered mesoporous structure and high specific surface area. The developed and ordered mesoporous structure effectively promotes the migration and diffusion of gas reactants and products in the CeCu–HT catalyst pore channels, thus providing a favorable condition for reactant molecule adsorption and product molecule desorption on the catalyst surface. The utilization rate of the catalyst inner surface also increases. Moreover, the large specific surface area of the CeCu–HT catalyst increases the contact area and the probability of contact between the reactant molecules and the catalyst. This particular phenomenon improves the

adsorption and activation ability of the CeCu–HT catalyst for reactant gas molecules, including O_2 gas and phenyl VOC molecules. By contrast, the aggregated structures and low porosities of the CeCu–PC and CeCu–CA catalysts weaken their adsorption ability for gas molecules. Their low specific surface areas also decrease the contact area and the probability of contact with reactant molecules. These features are responsible for the occurrence of reactant molecule adsorption and activation mainly on the outer surfaces of the CeCu–PC and CeCu–CA catalysts. Thus, the utilization rates of the active components of these catalysts are not significantly improved. The abilities of the CeCu–PC and CeCu–CA catalysts to activate reactant molecules are greatly weakened and lead to significantly reduced catalytic performances. Therefore, the superior phenyl VOC catalytic combustion activity of the CeCu–HT catalyst can also be attributed to its superior structural properties.

Fig.s 5a to 5c show that toluene, ethylbenzene, xylene, and benzene exhibit significantly different catalytic combustion activity orders over the CeCu–HT, CeCu–PC, and CeCu–CA catalysts. The phenyl VOC reactant molecules all have a benzene ring in their basic structure. Moreover, toluene, ethylbenzene, and xylene are obtained through the substitution of the hydrogen atom on the benzene ring by a methyl or ethyl group. Ethyl and methyl substituents are electron-contributing groups that significantly affect the π electronic structure and charge density distribution of the benzene ring. Therefore, the addition of these groups disrupts the symmetry and stability of the benzene ring. Although benzene molecules exhibit low ignition temperatures over the CeCu–HT and CeCu–PC catalysts, the catalytic combustion

conversion of benzene over the investigated samples is the lowest among the investigated phenyl VOCs in the studied reaction temperature range. This result can be attributed to the aromatic ring structure of the molecule itself. The high symmetry and stability of the benzene ring result in high stability during catalytic combustion. Given the big group structure and strong electronic effect of the ethyl group, the symmetry and stability of the benzene ring structure of ethylbenzene are severely destroyed. Thus, ethylbenzene exhibits higher catalytic combustion catalyst activity over the CeCu–HT, CeCu–PC, and CeCu–CA catalysts. CeCu–HT has a developed and ordered mesoporous structure. Generally, reactants with small molecular sizes migrate and diffuse more easily in the pore channels of catalysts than the larger ones. Small-molecule reactants can therefore be adsorbed and activated more easily by the active centers on the catalyst inner pore wall, which results in high catalytic activity. The molecular sizes of benzene, toluene, and xylene are 4.97, 5.83, and 6.68 Å, respectively.[29] These molecular sizes follow the catalytic light-off temperature order of benzene > toluene > xylene over the CeCu–HT catalyst, which is consistent with the molecular size sequence. In flow gas reaction systems, the small molecular size of benzene is favorable for the desorption of adsorbed benzene molecules from the porous catalyst structure, thus decreasing the adsorption and activation ability of the catalyst for benzene molecules and hindering their complete combustion. Therefore, the small size and stable molecular structure of benzene can be the vital factor for its low catalytic combustion conversion (<70%) over the CeCu oxide catalysts. The results indicate that phenyl VOC catalytic combustion activity over the prepared

CeCu oxide catalysts is significantly affected by the chemical composition and structure of the catalysts, as well as by the physicochemical properties of the phenyl VOC molecules.

3.6 Determination of ethylbenzene catalytic combustion stability

The ethylbenzene catalytic combustion stability on the prepared CeCu–HT, CeCu–PC, and CeCu–CA catalysts at different reaction conditions are shown in Figs. 6a to 6c, respectively. Fig. 6a shows that the ethylbenzene removal over the CeCu–HT catalyst gradually decreases from 30% to 0 within 18 min at 215 °C. The ethylbenzene catalytic combustion conversion over the CeCu–HT catalyst exceeds 94% at 220 °C, and ethylbenzene conversion is maintained above 89% within 116 min. However, ethylbenzene conversion starts to decline clearly when the reaction time walks 116 min. And ethylbenzene conversion decreases to about 27% at a reaction time of approximately 301 min, during which the ethylbenzene conversion is stable at about 42% for 70 min from about 182 to 251 min. When the reaction temperature reaches 230 °C, the ethylbenzene catalytic combustion conversion is 100% at the initial stage and gradually decreases to 98% within 16 min. Afterward, the CeCu–HT catalyst shows high stability for ethylbenzene catalytic combustion. The ethylbenzene catalytic combustion conversion remains constantly above 95% within 604 min. The reaction condition is changed by using N_2 as a substitute for air and completely removing air from the reaction system. The feed gas is then switched to a mixture of N_2 and ethylbenzene (ethylbenzene 1.0 vol% and N_2 99 vol%) at a reaction temperature of 230 °C. The ethylbenzene catalytic conversion over the

CeCu–HT catalyst gradually decreases from about 45% to 0 within 22 min. However, the ethylbenzene conversion is zero in the absence of CeCu-HT catalyst. Fig. 7b shows that the ethylbenzene removal over the CeCu–PC catalyst rapidly decreases from 13% to 0% within 9 min at 225 °C. At 230 °C, the ethylbenzene catalytic combustion conversion over the CeCu–PC catalyst gradually decreases from 97% at the initial stage to 92% within 14 min, then it remains at approximately 92%. Fig. 7c shows that the ethylbenzene over the CeCu–CA catalyst gradually decreases from 14% to 0% within 8 min at 240 °C. At 245 and 250°C, the ethylbenzene conversion over CeCu–CA gradually decreases from 73% and 75% to about 46% and 52% as the reaction time walks 600 min, respectively. At 260 °C, the ethylbenzene conversion over CeCu–CA rapidly decreases from 93% at the initial stage to 80% within 10 min. Subsequently, the ethylbenzene catalytic combustion conversions remain at above 75% within 600 min. When N_2 gas is substituted for air, the ethylbenzene removal over CeCu-PC and CeCu–CA gradually decrease from 31% and 24% to approximately zero within 10 min, respectively.

Meanwhile, ethylbenzene combustion does not occur on the CeCu–HT, CeCu–PC and CeCu–CA catalysts at 215 °C, 220 °C and 240 °C, respectively. Although the initial ethylbenzene removals on the CeCu–HT, CeCu–PC, and CeCu–CA catalysts reach 30%, 13%, and 14%, respectively, these results may primarily be attributed to the adsorption of ethylbenzene molecules on the catalysts. The low adsorption performance of the CeCu–PC catalyst for ethylbenzene may be closely related to its large-particle, aggregated structure. By comparison, the

adsorption performance on the CeCu–CA catalyst improves as the particle size decreases and the specific surface area increases. The CeCu–HT catalyst has a high adsorption performance for ethylbenzene, which is essentially related to the developed mesoporous structure and large specific surface area of the catalyst, as determined by TEM and BET analyses. Moreover, the high ethylbenzene adsorption performance of the CeCu–HT catalyst is conducive to the effective activation of ethylbenzene molecules. Ethylbenzene conversion is zero when the catalytic reaction system has no catalyst. This result indicates that ethylbenzene cannot be removed through direct combustion at low temperatures unless a high-performance catalyst is introduced in the reaction system. Based on these results, the gaseous oxygen molecules do not directly participate in catalytic combustion reactions. These molecules usually achieve high catalytic oxidation or combustion activity only after being activated by the catalysts to form reactive oxygen species.[30] The XPS results show that the CeCu–HT catalyst has higher content of reactive oxygen species than the CeCu–PC and CeCu–CA catalysts, which can directly participate in the catalytic oxidation or combustion reaction of organic molecules under certain conditions.[31] However, ethylbenzene conversions over the CeCu-HT, CeCu–PC and CeCu–CA catalysts at 230, 230, and 240 °C under an inert atmosphere reach 45%, 31%, and 24%, respectively. This result can be attributed to the small amount of active oxygen species directly participating in the ethylbenzene catalytic combustion and to the adsorption of ethylbenzene on the catalysts. The phenomenon on CeCu-HT is different with that toluene conversion over CeCu-HT exceeds 80% under the inert

atmosphere.[13] The reason may be that ethylbenzene combustion needs more reactive oxygen species than toluene combustion. When the catalytic reaction is performed at 230 °C in air, the CeCu–HT catalyst maintains a high and stable ethylbenzene catalytic combustion conversion. By contrast, the CeCu–PC and CeCu–CA catalysts maintain high and stable ethylbenzene catalytic combustion conversions at 230 and 260 °C, respectively. This result demonstrates that the O_2 molecules in air can be activated by the catalysts to form active oxygen species that can effectively replace the consumed ones during the ethylbenzene catalytic combustion. As the ethylbenzene catalytic combustion reaction being performed at 225 °C over CeCu–HT the ethylbenzene conversion gradually decreases after the reaction exceeds certain minutes, which is similar with toluene combustion over this catalyst.[13] This decreased activity indicates that the CeCu–HT catalyst begins to deactivate, the same happened to CeCu-CA. The reactive oxygen species in the CeCu–HT catalyst are gradually consumed for ethylbenzene catalytic combustion, and the gaseous oxygen molecules in the air cannot be effectively activated by the CeCu–HT CeCu-CA catalysts at corresponding reaction temperatures. As a result, the consumed reactive oxygen species in the CeCu–HT and CeCu-CA catalysts cannot obtain an effective supplement during ethylbenzene catalytic combustion, resulting in a lower "supply" of reactive oxygen species compared with the "consumption" in the ethylbenzene catalytic reaction system. Therefore, the ethylbenzene catalytic combustion activity on the CeCu–HT CeCu-CA catalysts clearly decreases after a certain period. In Fig. 6, the investigated CeCu oxide catalysts all exhibit high ethylbenzene conversion at the

initial stage of the reaction under the corresponding high temperatures and the conversion slightly decrease in several minutes. The high ethylbenzene conversion at the initial stage of the reaction can be attributed to the functions of the reactive oxygen species on the CeCu oxide catalyst surfaces during ethylbenzene catalytic combustion and to the adsorption of ethylbenzene on the CeCu oxide catalysts. Moreover, the slight decline in ethylbenzene conversion can be attributed to the consumption of large amounts of reactive oxygen species on the CeCu oxide catalyst surfaces. When the reaction temperature increases to 230 and 260°C, the energy of the reaction system increases and promotes the activation of gaseous O_2 molecules to form reactive oxygen species on the CeCu–HT and CeCu-CA catalysts, respectively. Thus, the CeCu–HT and CeCu-CA catalysts can continuously provide abundant reactive oxygen species for ethylbenzene catalytic combustion and guarantee the "consumption" of the active oxygen species to maintain the balance with the "supply". Therefore, the CeCu–HT catalyst shows high ethylbenzene catalytic combustion performance and stability at 230 °C, and thus, has high potential application in phenyl VOC removal in air.

4. Conclusions

The physical and chemical performances of CeCu composite oxide catalysts can be affected by preparation methods. The CeCu–HT catalyst has large specific surface area of 206 $m^2 \cdot g^{-1}$ and an ordered mesoporous structure with an aperture of 5 nm to 6 nm. And it has a uniform CeO_2–CuO oxide solid solution phase with high

metal–oxide dispersion. However, the CeCu–PC and CeCu–CA catalysts have large particles with low-porosity structures and low specific surface areas of less than 24 $m^2 \cdot g^{-1}$. The CeCu–HT catalyst has higher reactive oxygen species content, better reducibility, and higher phenyl VOC catalytic combustion activity than the CeCu–PC and CeCu–CA catalysts. The phenyl VOC catalytic combustion activity on the CeCu–HT catalyst follows the order ethylbenzene > toluene > xylene > benzene. The differences between the phenyl VOC catalytic combustion performances of the CeCu–HT, CeCu–PC, and CeCu–CA catalysts can be attributed to their different surface chemical compositions and structures. The prepared CeCu oxide catalysts show high activities and stabilities for ethylbenzene catalytic combustion. The CeCu–HT catalyst, which has superior chemical components, large specific surface area and developed ordered mesoporous structure, has high potential application in the removal of phenyl VOCs from air.

Acknowledgements

The work was financially supported by Project from Science and Technology of Chongqing Municipal Education Commission funded research projects (KJ1400610); Project of Chongqing Hundred Leaders in Talent Cultivation Plan of Academic Discipline; Natural Science Foundation Project of CQ CSTC (CSTC, 2011jjA2008).

Reference

1 Y. Liu, M. Shao, L. L. Fu, S. H. Lu, L. M. Zeng and D. G. Tang, *Atmos. Environ.*,

2008, **42**, 6247.

2 G. L. Zhou, H. Lan, H. Wang, H. M. Xie, G. Z. Zhang, X. X. Zheng, *J. Mol. Catal. A: Chem.*, 2014, **393**, 279.

3 T. Tsoncheva, G. Issaa, T. Blasco, M. Dimitrov, M. Popova, S. Hernández, D. Kovacheva, G. Atanasova and J. M. L. Nieto, *Appl. Catal. A: Gen.*, 2013, **453**, 1.

4 H. F. Lu, Y. Zhou, W. F. Han, H. F. Huang and Y. F. Chen, *Catal. Sci. Technol.*, 2013, **3**, 1480.

5 X. M. Qi and M. Flytzani–Stephanopoulos, *Ind. Eng. Chem. Res.*, 2004, **43**, 3055.

6 Z. G. Liu, R. X. Zhou and X. M. Zheng, *Catal. Commun.*, 2008, **9**, 2183.

7 W. J. Shan, Z. C. Feng, Z. G. Li, J. Zhang, W. J. Shen and C. Li, *J. Catal.*, 2004, **228**, 206.

8 H. B. Zhou, Z. Huang, C. Sun, F. Qin, D. S. Xiong, W. Shen and H. L. Xu, *Appl. Catal. B*, 2012, **125**, 492.

9 C. Q. Hua, Q. S. Zhua, Z. Jiang, L. Chen and R. F. Wu, *Chem. Eng. J.*, 2009, **152**, 583.

10 F. X. Yin, S. F. Ji, N. Z. Chen, M. L. Zhang, L. P. Zhao, C. Y. Li and H. Liu, *Catal. Today*, 2005, **105**, 372.

11 S. C. Laha and R. Ryoo, *Chem. Commun.*, 2003, **17**, 2138.

12 A. Rumplecker, F. Kleitz, E. L. Salabas and F. Schüth, *Chem. Mater.*, 2007, **19**, 485.

13 G. L. Zhou, H. Lan, T. T. Gao and H. M. Xie, *Chem. Eng. J.*, 2014, **246**, 53.

14 F. Kleitz, S. H. Choi and R. Ryoo, *Chem. Commun.*, 2003, **17**, 2136.

15 J. Rebellato, M. M. Natile and A. Glisenti, *Appl. Catal. A*, 2008, **339**, 108.

16 Z. Y. Fei, P. Lu, X. Z. Feng, B. Sun and W. J. Ji, *Catal. Sci. Technol.*, 2012, **2**, 1705.

17 V. M. L. Whiffena, K. J. Smitha and S. K. Straus, *Appl. Catal. A*, 2012, **419–420**, 111.

18 P. Djinović, J. Batista, J. Levec and A. Pintar, *Appl. Catal. A*, 2009, **364**, 156.

19 G. L. Zhou, Ti. Wu, H. M. Xie and X. X. Zheng. *Int. J. Hydrogen Eng.*, 2013, **38**, 10012.

20 K. S. W. Sing, D. H. Everett, R. A. W. Haul, L. Moscou, R. A. Pierott and J. Rouquerol, *Pure Appl. Chem.*, 1985, **57**, 603.

21 C. L. Guo, X. L. Zhang, J. L. Zhang and Y. P. Wang, *J. Mol. Catal. A*, 2007, **269**, 254.

22 F. Jiao, A. Harrison, A. H. Hill and P. G. Bruce, *Adv. Mater.*, 2007, **19**, 4063.

23 L. Jiang, H. W. Zhu, R. Razzaq, M. L. Zhu, C. S. Li and Z. X. Li, *Int. J. Hydrogen Eng.*, 2012, **37**, 15914.

24 S. Ponce, M. A. Peña and J. L. G. Fierro, *Appl. Catal. B: Environ.*, 2000, **24**, 193.

25 M. W. Ryoo, S. G. Chung, J. H. Kim, Y. S. Song and G. Seo, *Catal. Today*, 2003, **83**, 131.

26 M. Guisnet, P. Dégé and P. Magnoux, *Appl. Catal. B: Environ.*, 1999, **20**, 1.

27 T. Mitsui, K. Tsutsui, T. Matsui, R. Kikuchi and K. Eguchi, *Appl. Catal. B: Environ.*, 2008, **81**, 56.

28 Q. H. Xia, K. Hidajat and S. Kawi, *Catal. Today*, 2001, **68**, 255.

29 K. J. A. Raj, E. J. P. Malar and V. R. Vijayaraghavan, *J. Mol. Catal. A*, 2006, **243**, 99.

30 G. Avgouropoulos and T. Ioannides, *Chem. Eng. J.*, 2011, **176–177**, 14.

31 A. P. Jia, G. S. Hu, L. Meng, Y. L. Xie, J. Q. Lu and M. F. Luo, *J. Catal.*, 2012, **289**, 199.

Table and Fig.s Captions:

Table 1 XPS and AAS analysis results of the prepared CeCu oxide catalysts

Fig. 1 XRD patterns of the CeCu-HT, CeCu-PC, CeCu-CA catalysts and KIT-6 template

Fig. 2. TEM images of the CeCu-HT, CeCu-PC, CeCu-CA catalysts and KIT-6 template

Fig. 3 XPS spectra of Ce 3d(a), Cu 2p (b), and O 1s (c) for the CeCu-HT, CeCu-PC and CeCu-CA catalysts

Fig. 4 The H_2–TPR profiles for the CeCu-HT, CeCu-PC, and CeCu-CA catalysts

Fig. 5a Relationship between reaction temperature and phenyl VOCs catalytic combustion conversion on the CeCu-HT catalyst

Fig. 5b Relationship between reaction temperature and phenyl VOCs catalytic combustion conversion on the CeCu-PC catalyst

Fig. 5c Relationship between reaction temperature and phenyl VOCs catalytic combustion conversion on the CeCu-CA catalyst

Fig. 6a Relationship between reaction time and ethylbenzene catalytic combustion conversion on the CeCu-HT catalyst

Fig. 6b Relationship between reaction time and ethylbenzene catalytic combustion conversion on the CeCu-PC catalyst

Fig. 6c Relationship between reaction time and ethylbenzene catalytic combustion conversion on the CeCu-CA catalyst

Table 1 XPS and AAS analysis results of the prepared CeCu oxide catalysts

Catalysts	Ce/Cu (AAS)	Ce/Cu (XPS)	Species	Percent / %
CeCu-PC	8.55	1.89	O_{Latt}	63.8
			O_{OH}	29.0
			O_{ads}	7.17
CeCu-CA	3.21	2.06	O_{Latt}	64.7
			O_{OH}	28.0
			O_{ads}	7.31
CeCu–HT	3.53	1.84	O_{Latt}	52.7
			O_{OH}	33.1
			O_{ads}	14.3

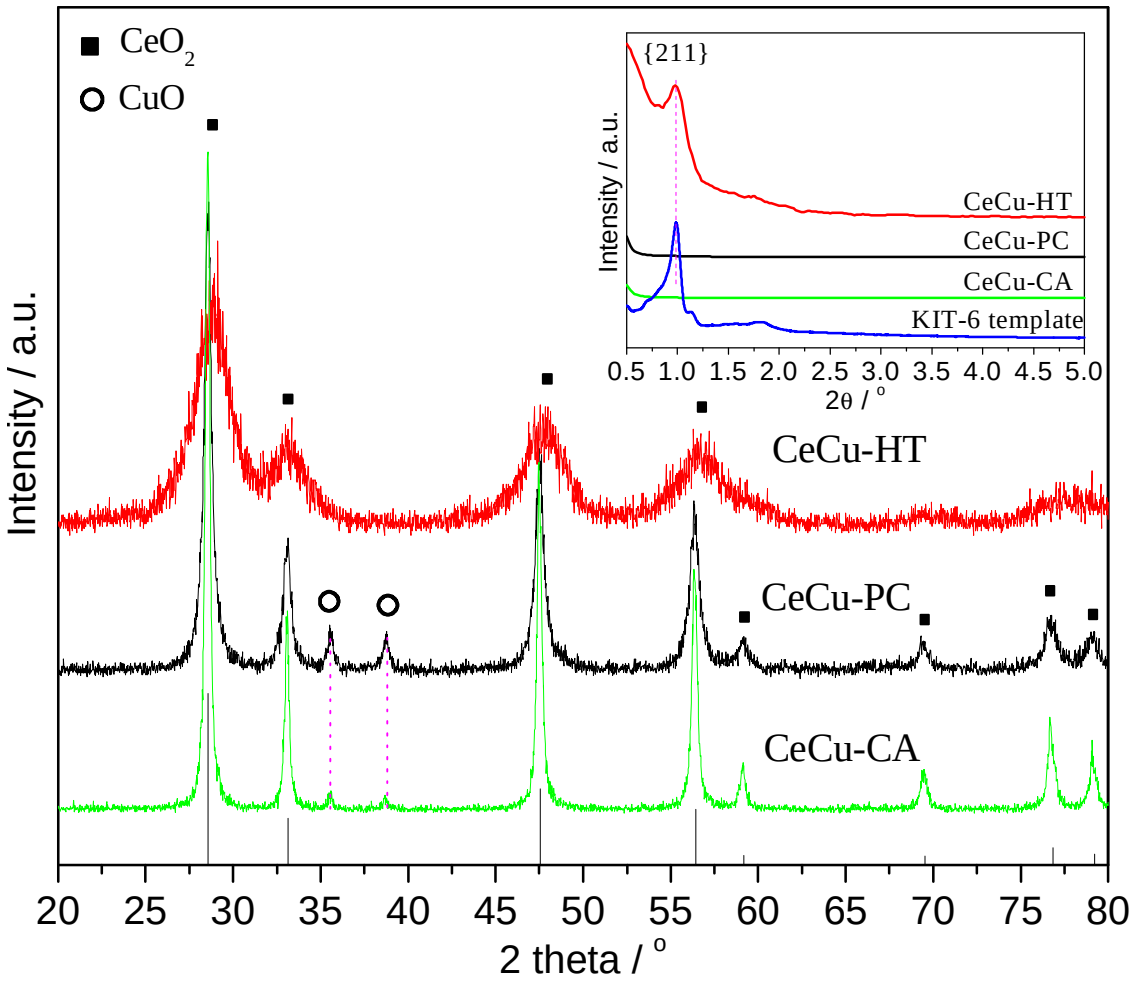

Fig. 1 XRD patterns of the CeCu-HT, CeCu-PC, CeCu-CA catalysts and KIT-6 template

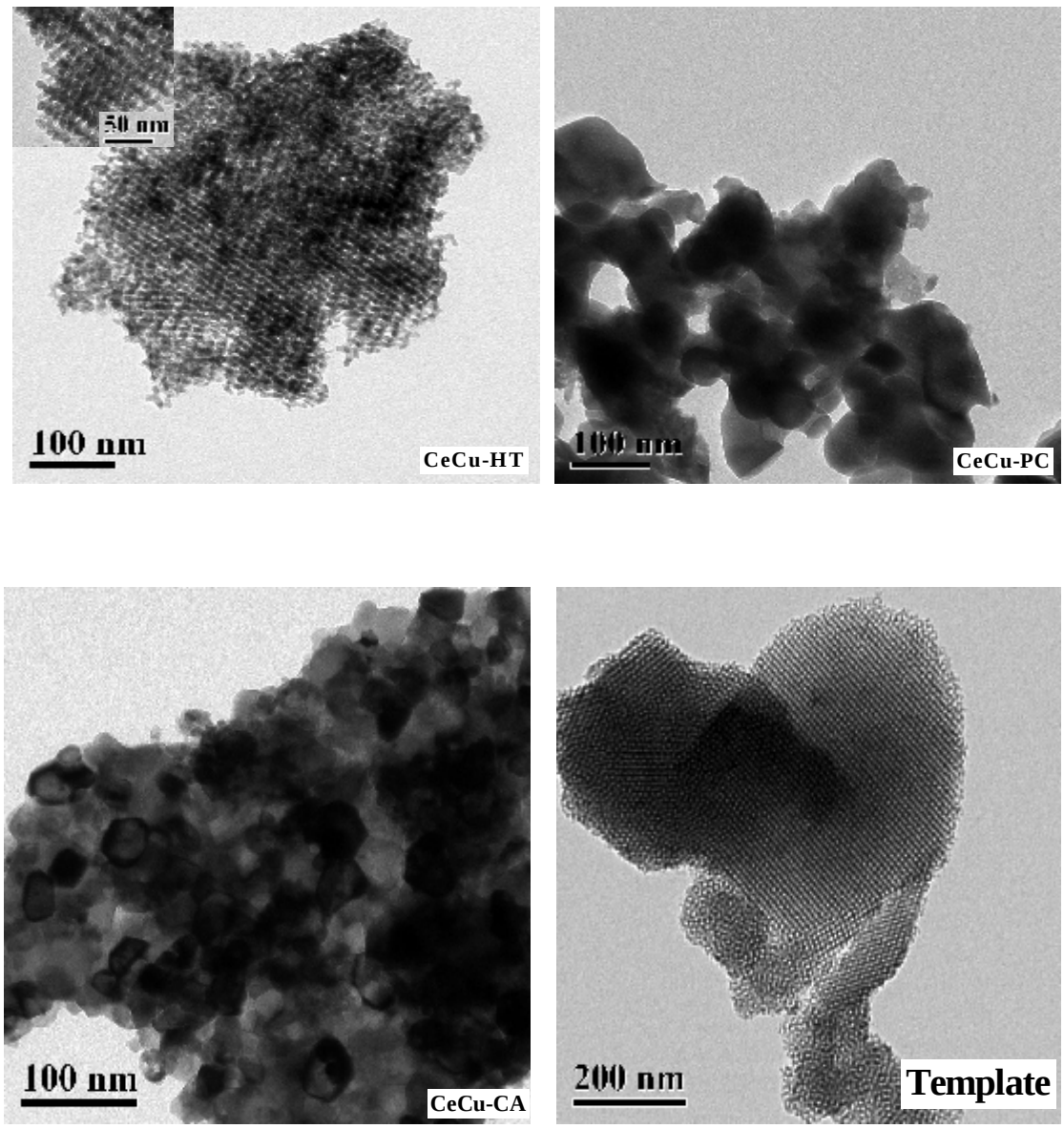

Fig. 2. TEM images of the CeCu-HT, CeCu-PC, CeCu-CA catalysts and KIT-6 template

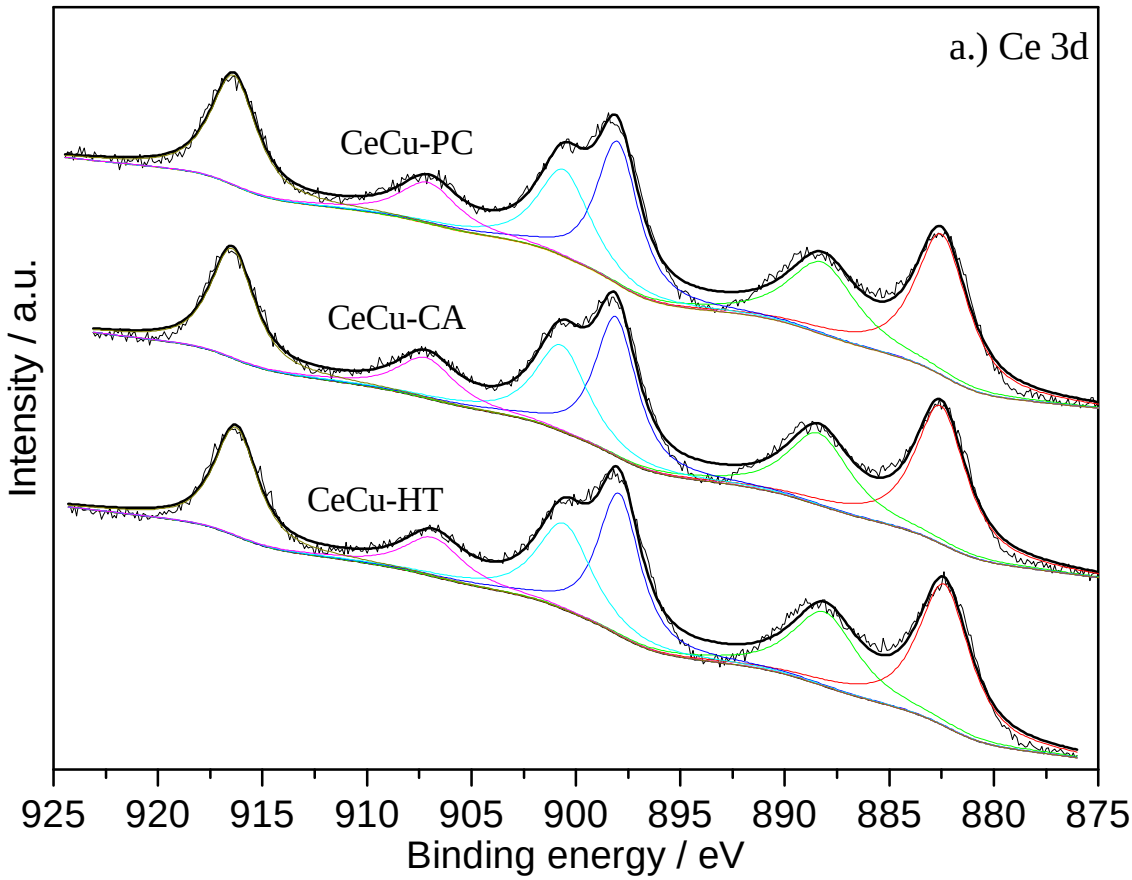

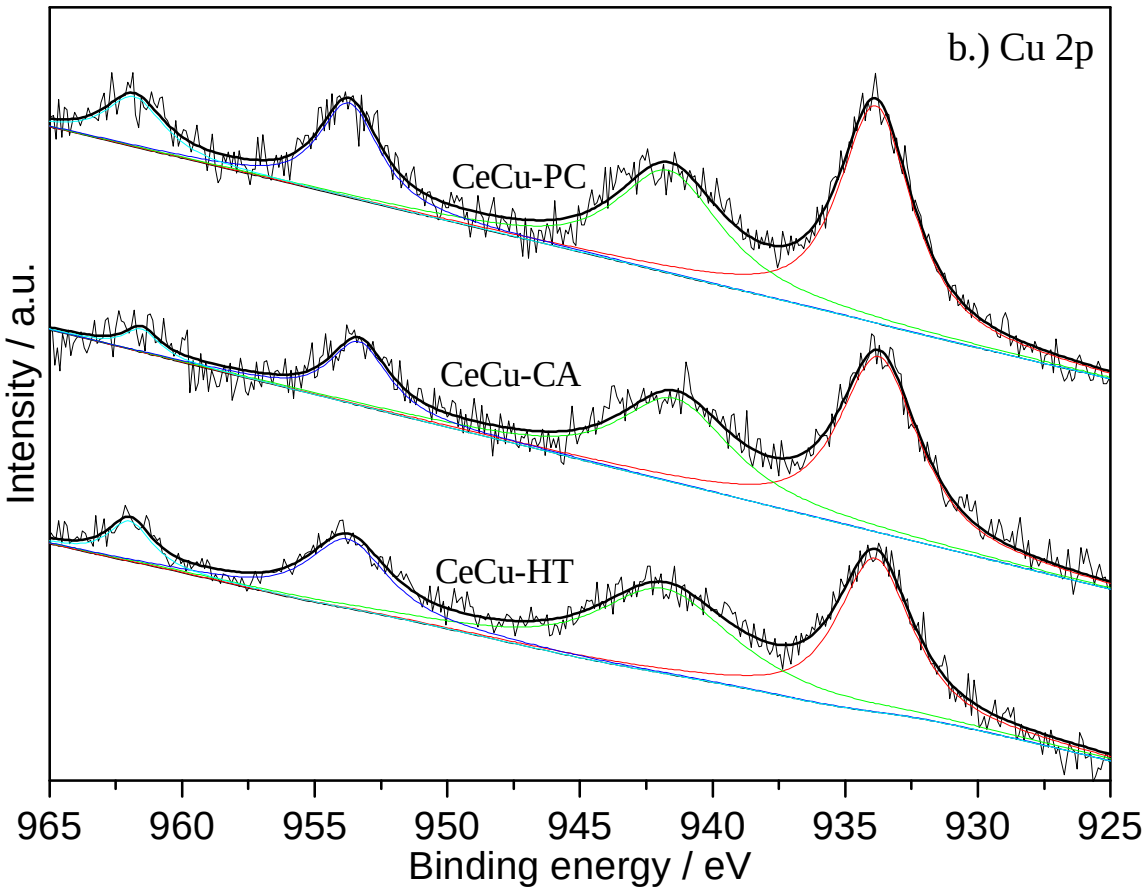

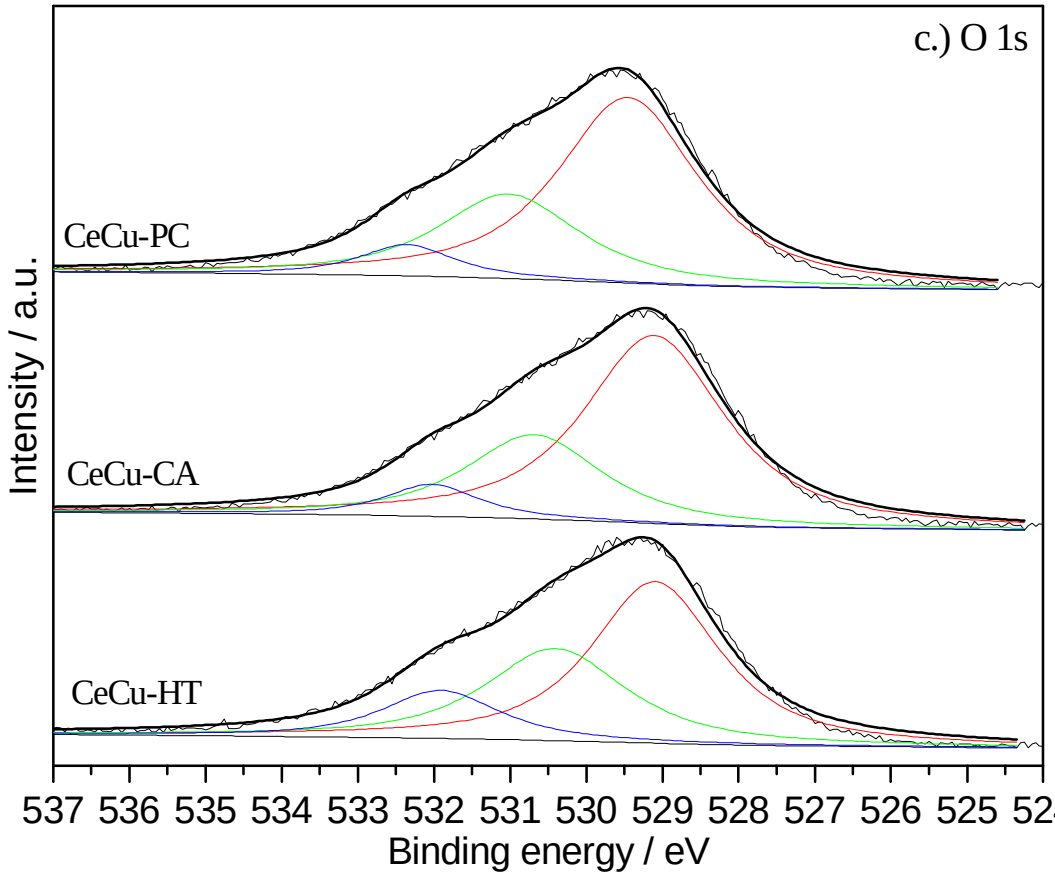

Fig. 3 XPS spectra of Ce 3d (a), Cu 2p (b), and O 1s (c) for the CeCu-HT, CeCu-PC, and CeCu-CA catalysts

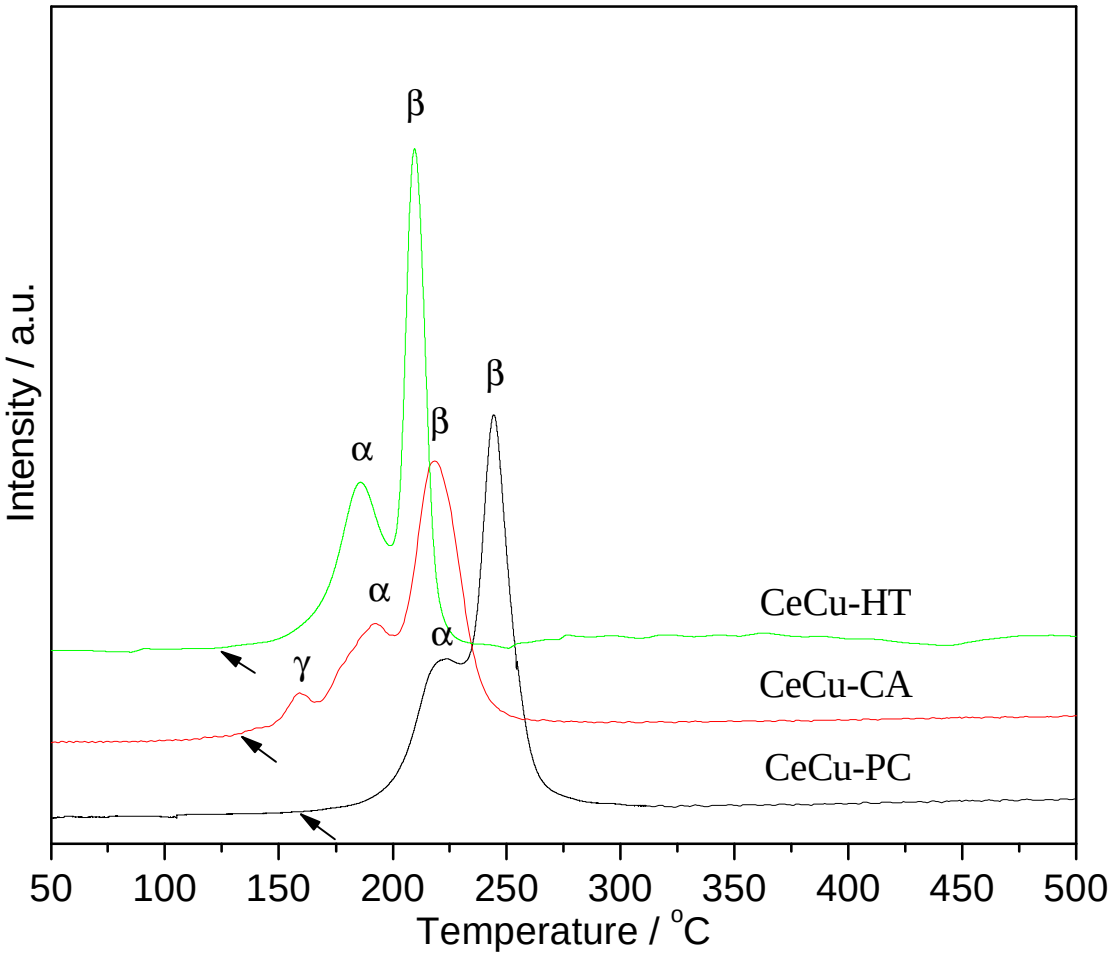

Fig. 4 The H_2–TPR profiles for the CeCu-HT, CeCu-PC, and CeCu-CA catalysts

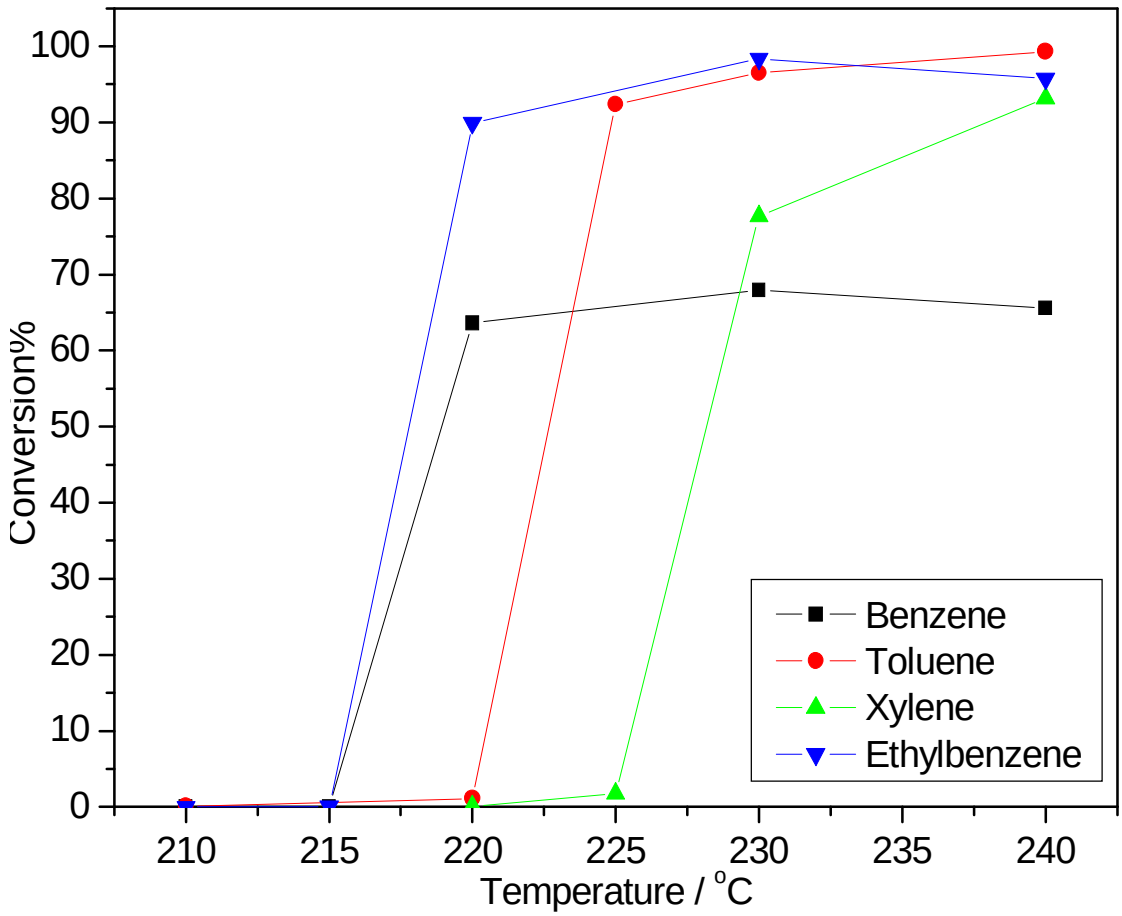

Fig. 5a Relationship between reaction temperature and phenyl VOCs catalytic combustion conversion on the CeCu-HT catalyst

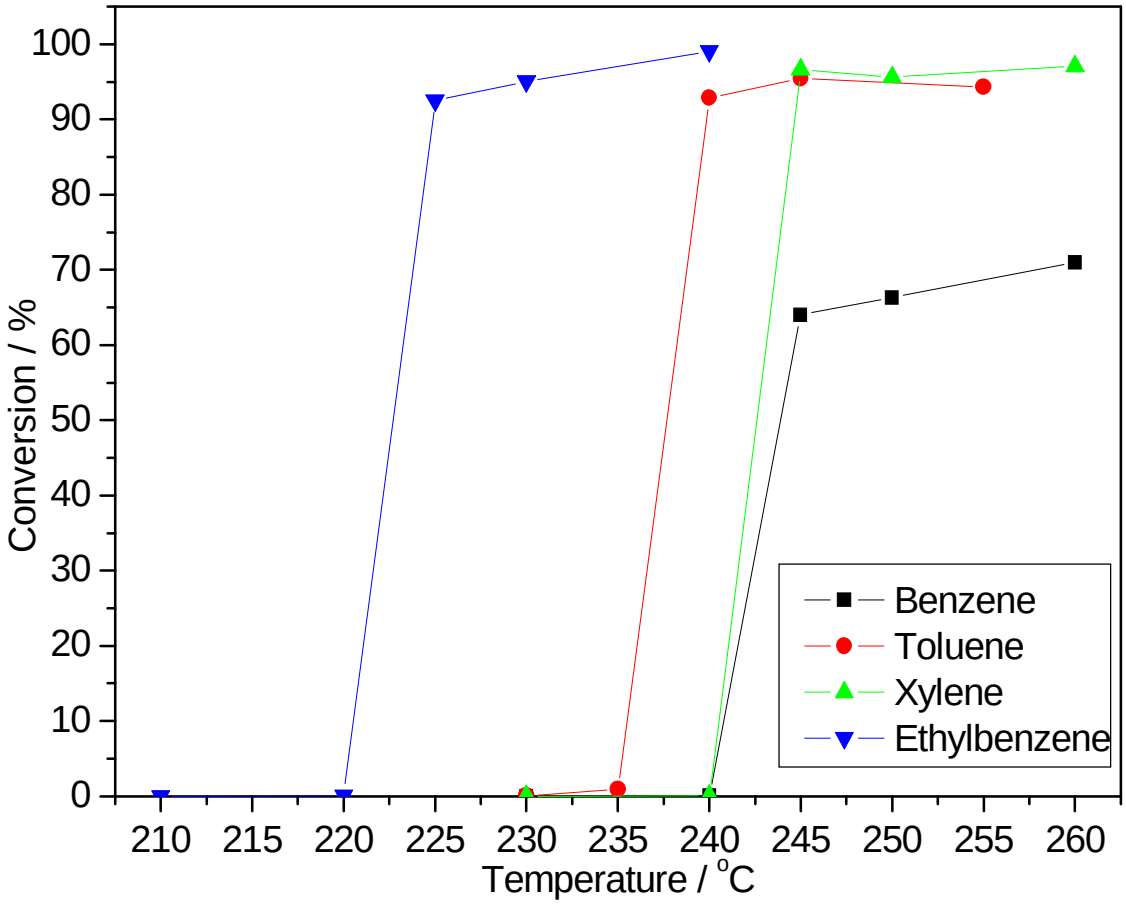

Fig. 5b Relationship between reaction temperature and phenyl VOCs catalytic combustion conversion on the CeCu-PC catalyst

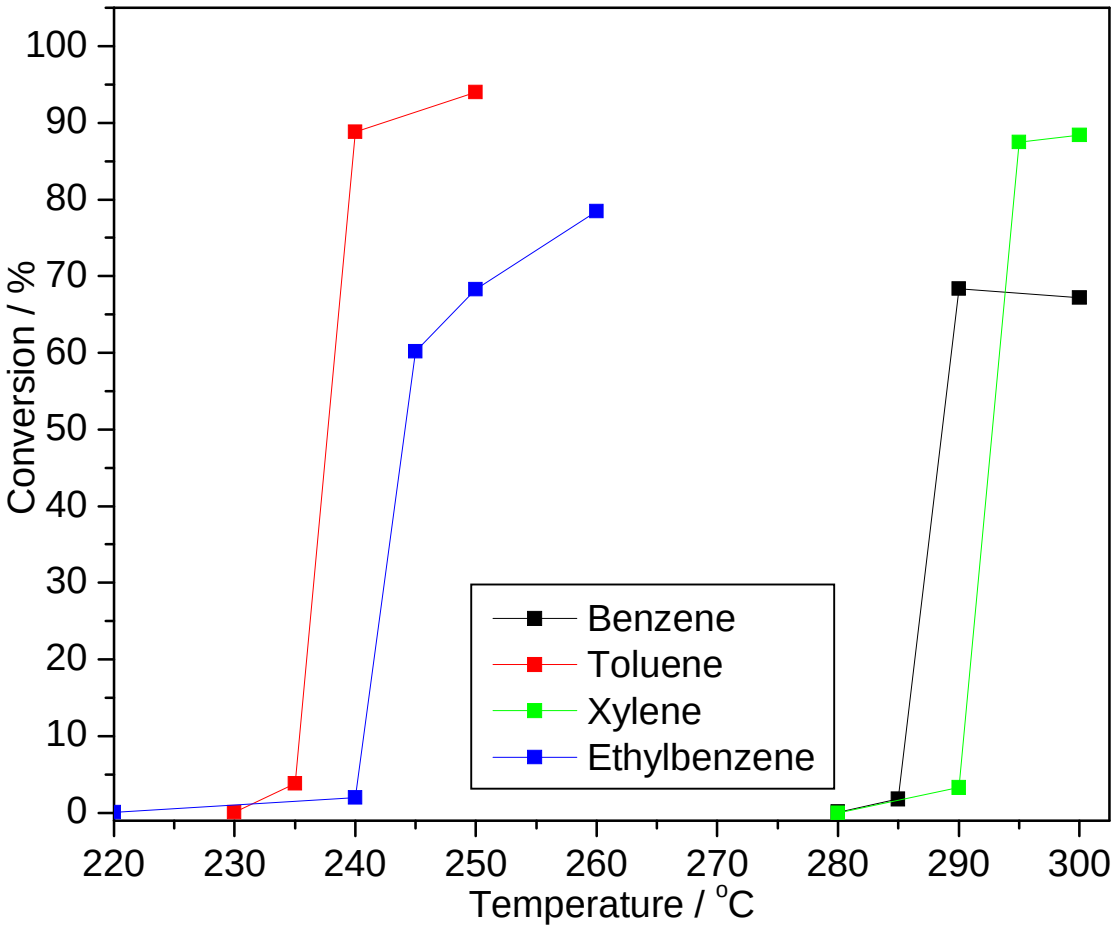

Fig. 5c Relationship between reaction temperature and phenyl VOCs catalytic combustion conversion on the CeCu-CA catalyst

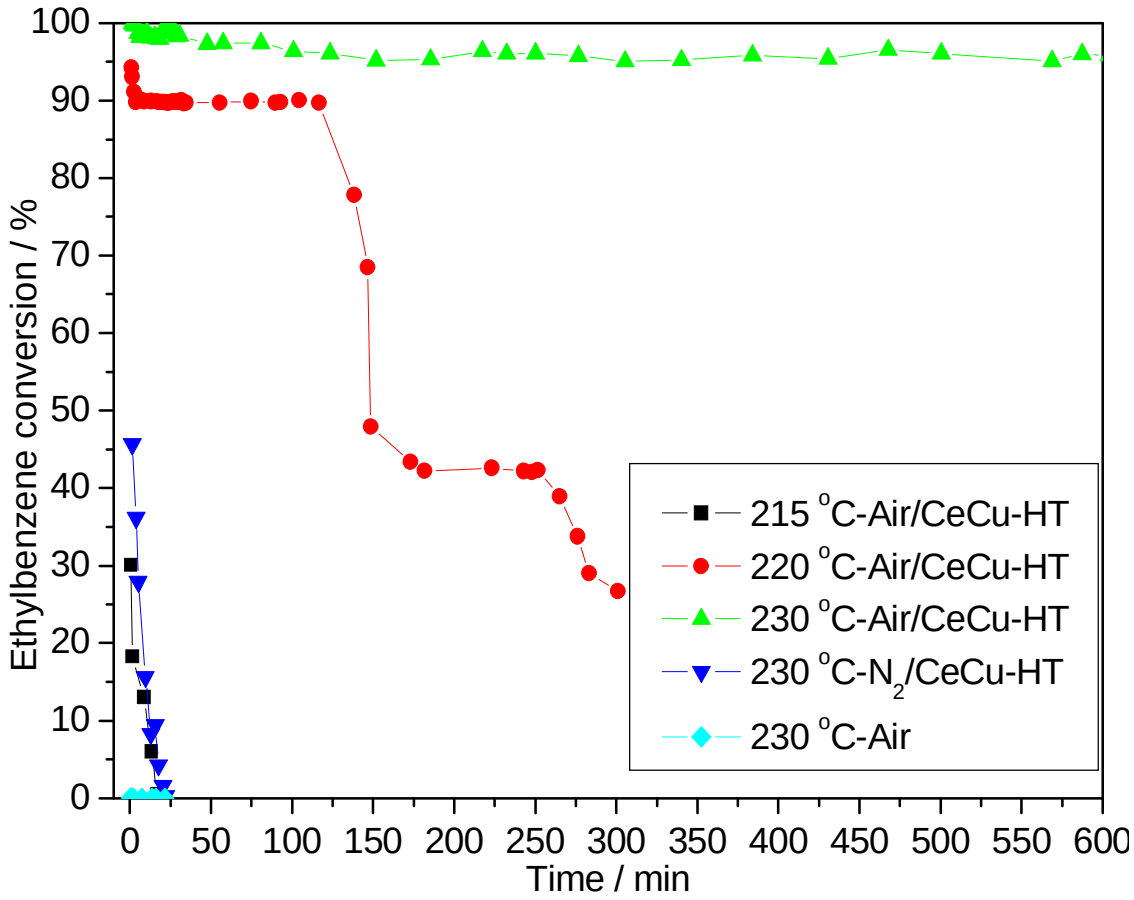

Fig. 6a Relationship between reaction time and ethylbenzene catalytic combustion conversion on the CeCu-HT catalyst

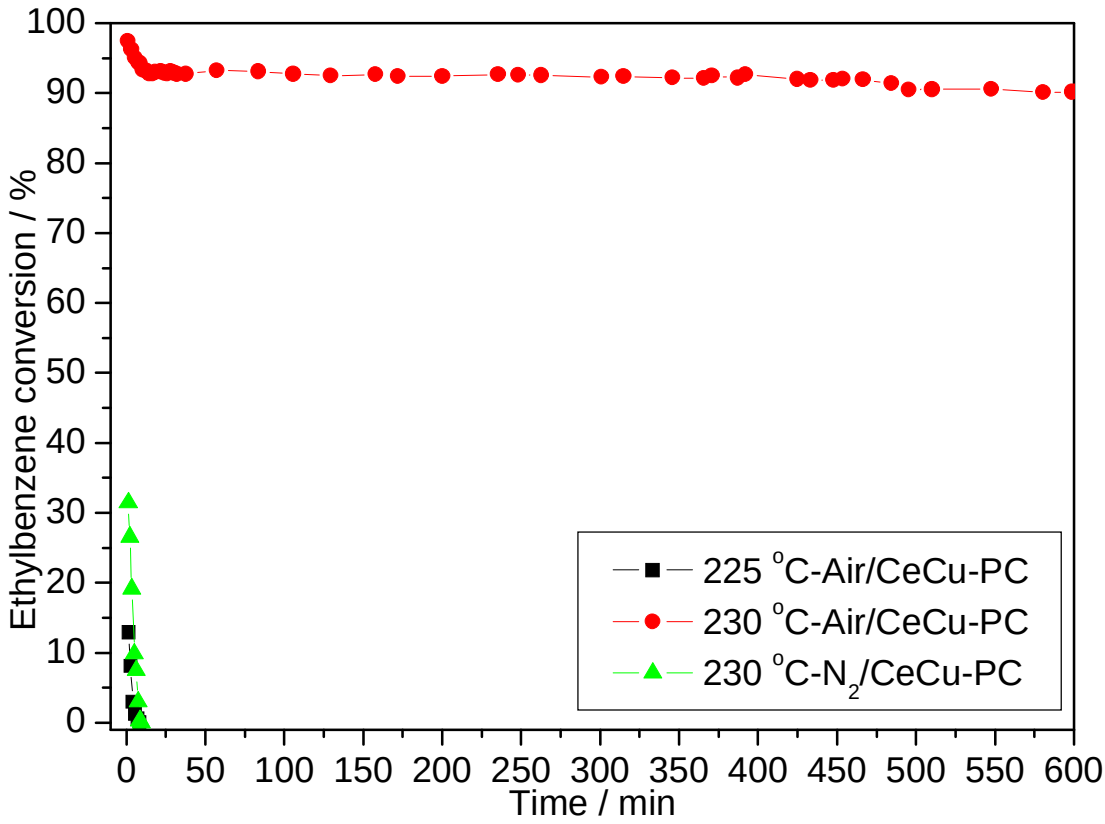

Fig. 6b Relationship between reaction time and ethylbenzene catalytic combustion conversion on the CeCu-PC catalyst

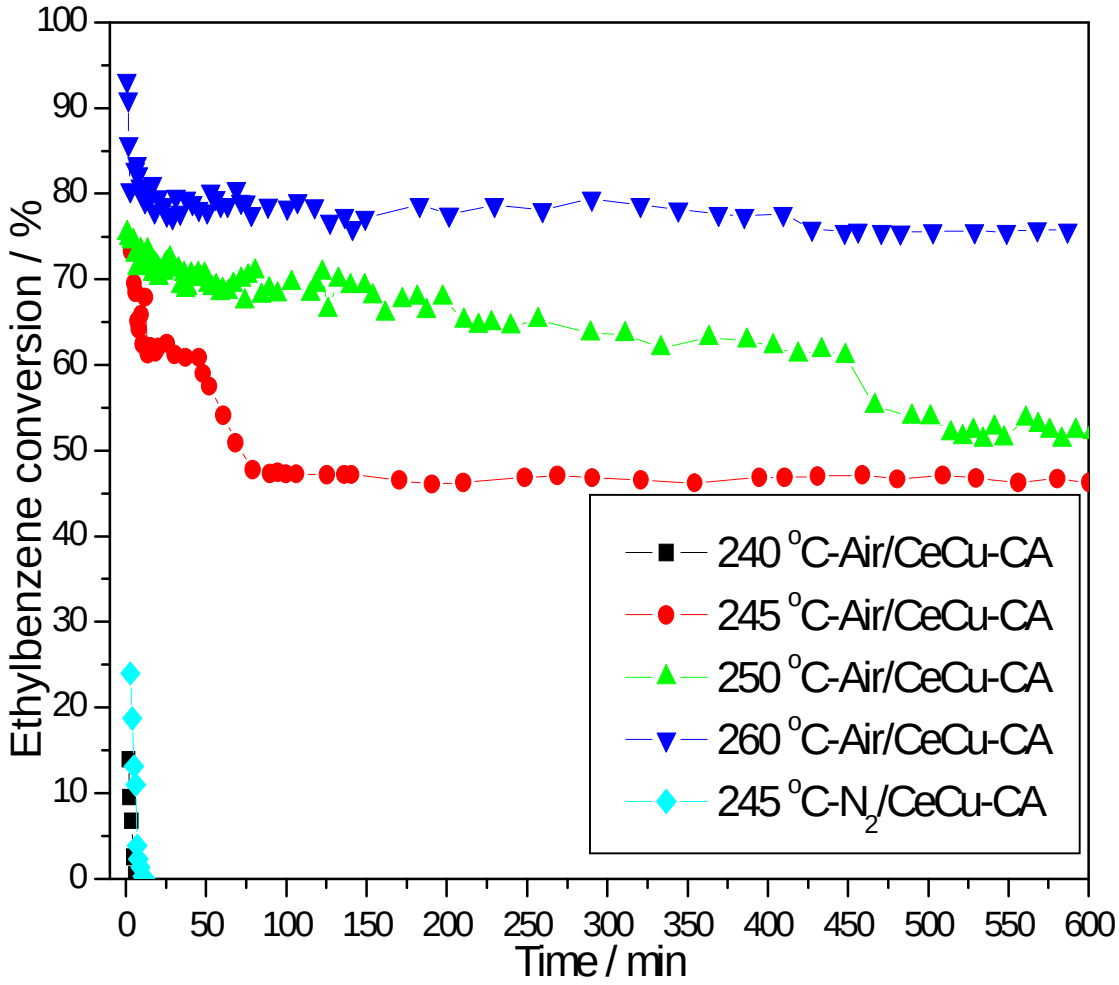

Fig. 6c Relationship between reaction time and ethylbenzene catalytic combustion conversion on the CeCu-CA catalyst